Period Determination and Classification Analysis of 25 Pulsating Red Giants

Anshita Saini
5246 145th Place SE, Bellevue, WA 98006; anshitasaini@gmail.com

Nicholas Walker
9808 Hillgreen Place, Beverly Hills, CA 90212; nickwalker106@gmail.com

Received February 6, 2021; revised February 28, March 5, 2021; accepted March 5, 2021

Abstract In this paper we present our updates and findings surrounding both period and classification analysis of 21 Miras and 4 semiregular variable stars. Our primary methods for confirming pulsation period include both qualitative and quantitative examination of time series plots and light curves, along with cross-confirmation using publicly-accessible databases with over a hundred years of published data. Using the visual observations and the Johnson V data from the AAVSO, and with the help of the AAVSO's VStar software, we arrived at refined period values to confirm data published by the VSX. Somewhat substantial updates are recommended for T UMi, from a period of 115.7 days to a primary and secondary period of 237.5 and 247.6 days, though no other variables merited such sizable adjustments. Finally, the application of self-correlation analysis provided further insight into the cycle-to-cycle changes in period and magnitude of semiregular variables.

1. Introduction

Pulsating red giants (PRGs) are radially-pulsating variable stars that occupy the ascending portion of the giant branch, along with the asymptotic giant branch (AGB), of the Hertzsprung-Russell Diagram. Stellar pulsation is typically caused by the expansion and contraction of the outer layers of such stars. Variables are classified according to factors like magnitude change and regularity of periodicity, the latter being the primary determinant of the *General Catalogue of Variable Stars* (GCVS; Samus *et al.* 2017) variability type. Mira variables, which have stellar features like those of the prototype Mira, o Ceti, have well-defined periods of around 100 to several hundred or up to 1,000 days. These periods may "wander" over time, a behavior studied in depth by Percy and Qiu (2019), Percy and Fenaux (2019), and Blackham (2020), though most Miras have regular fundamental pulsation modes. Their magnitudes vary by 2.5 to 11 magnitudes in the visual waveband.

Semiregular (SR) variable stars display periodicity, but differ from Miras due to often ill-defined periods and characteristic irregularities. The periods of semiregular variable stars can range from 20 to over 2,000 days, nearly twice those of longer-period Mira stars. Light amplitudes of semiregular stars vary as well, ranging from several hundredths to several magnitudes (GCVS). The SR stars presented in this paper exhibit increasing or decreasing trends in light amplitude over time scales of several thousand Julian days.

Semiregular variable giants are additionally subdivided into subclasses of SRA, SRB, SRC, SRD, and SRS. SRA stars similarly demonstrate periodicity and changing amplitudes and often exhibit light curves similar to Miras. However, SRA stars have smaller light amplitudes with more consistent magnitudes—generally below 2.5 magnitudes in V. Ranging from 25 to 1,200 days, the periods of SRA stars align more closely to the range of Mira periods than to the full range of SR periods.

SRB stars display poorly-defined periodicity and irregularities, distinguishing them from SR and SRA variable stars. The GCVS assigns each SRB a mean period, though these stars often have two or more pulsating modes. The mean period range is similar to that of semiregular stars and ranges from 20 to 2,300 days.

This study aims to confirm the periods and classifications of several SR variable stars and Mira variables through various methods of analysis on visual observations. The 25 variables in our study were chosen primarily due to their location in constellations near the North Celestial Pole in order to limit seasonal gaps in their light curves. Beyond that rationale, the stars were chosen semi-arbitrarily, though the SR variables within some of these constellations were selected due to their relative abundance of photometric data. Quantitative analysis of periodicity is presented through Fourier analysis and the Analysis of Variance algorithm. The classification of these stars was confirmed through qualitative analysis of light curves and self-correlation plots.

2. Resources

2.1. Variable Star Index (VSX)

The International Variable Star Index (VSX), developed for working groups of the American Association of Variable Star Observers (AAVSO), currently catalogs around 2 million variable stars (Watson *et al.* 2014). Each star in the catalog is updated with peer-reviewed information on its position, aliases, variability type, spectral type, magnitude range, and period, as well as links to relevant academic references. Many of the stars discussed in this paper may warrant updates in the VSX, while others in the index have been recently revised.

2.2. AAVSO International Database (AID)

The American Association of Variable Star Observers' International Database (AAVSO's AID) contains nearly 50 million variable stars observations, including data points from over 100 years ago. The open-source database provided the visual and Johnson V band observational data used to analyze both semi-regular and Mira stars. As the largest and

most comprehensive variable star database of its kind, the AID contains thousands of thoroughly reviewed observations contributed by various organizations and amateur astronomers around the world (Kafka 2021).

2.3. VSTAR

The AAVSO's VSTAR data visualization tool was used for period and magnitude analysis of the 25 chosen variable stars. The open-source application allows the user to generate light curves using data queried from AAVSO AID, as well as data from a variety of file types. VSTAR additionally offers the option of generating phase plots based on a user-inputted period (Benn 2013). In addition to such plots, VSTAR offers multiple implementations of Discrete Fourier Transform analysis, including a "Standard Scan" or relying on a frequency or period range as provided by the user. Applying one of these three Fourier analysis options results in a "top hits" table, as well as a power spectrum (AAVSO 2018). VSTAR also provides an implementation of the Analysis of Variance (AoV) algorithm, with an accompanying "top hits" table and periodogram.

3. Methods

3.1. DC DFT

We applied the Date-Compensated Discrete Fourier Transform (DC DFT) algorithm (Ferraz-Mello 1981) in VSTAR to determine the periods of the variable stars presented in this paper. The DC DFT finds the Fourier coefficients assuming that a periodic model fits the light curve. VSTAR's date-compensated algorithm ensures that gaps in the data are accounted for, yielding accurate analysis on both well-sampled and poorly-observed stars.

The DC DFT also determines the power, or statistical significance, associated with the Fourier coefficients. The highest power levels indicate that the corresponding frequency is a likely candidate for the fundamental frequency of the data. These values are represented in the power spectra in Figures 1 and 2, with the x-axis as Frequency (Hertz) and the y-axis as the power of each frequency.

Figure 1 depicts the DC DFT plot of T UMi with two peaks of comparable powers. The secondary peak of 0.004039 Hz corresponds to a candidate secondary pulsation mode, present in many of the DC DFT plots of semiregular variables. The plots of most Mira stars were similar to the power spectrum of X Cep in Figure 2, although this plot also shows evident harmonic peaks at frequency intervals of 0.001850 Hz. This curve, along with those in Figures 2–4, was generated for the purpose of our analysis, though we include them here as examples of VSTAR's capabilities.

3.2. AoV

A second tool—Analysis of Variance (AoV)—was applied to confirm the period(s) found by DC DFT. Unlike Fourier analysis, this method relies on the One-way Analysis of Variance (ANOVA) algorithm to extract candidate periods. Upon inputting a period range based upon the DC DFT and the VSX periods, VSTAR's AoV algorithm computes an "F-statistic," a measure of statistical significance similar to the DC DFT power level for each candidate period.

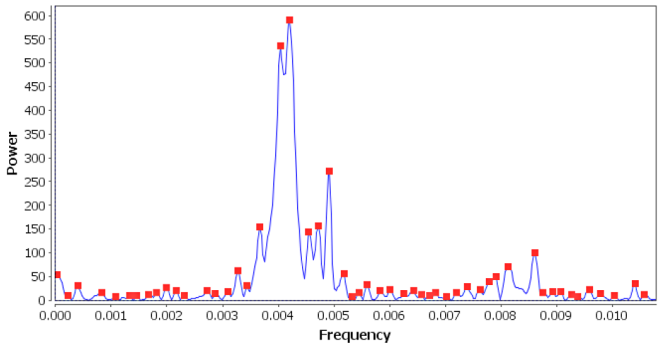

Figure 1. A power spectrum, or DC DFT plot, for SR variable T UMi (JD 2450000–JD 2459200).

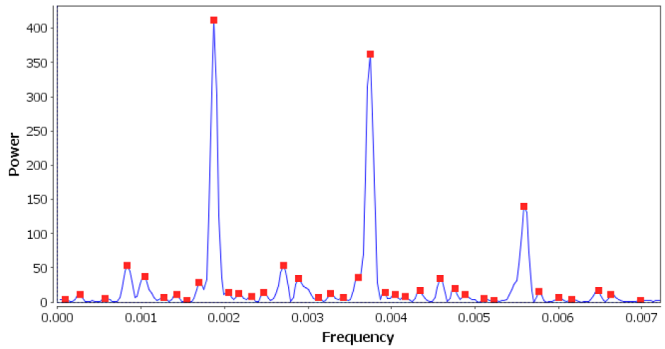

Figure 2. DC DFT plot for Mira X Cep (JD 2450000–JD 2459200).

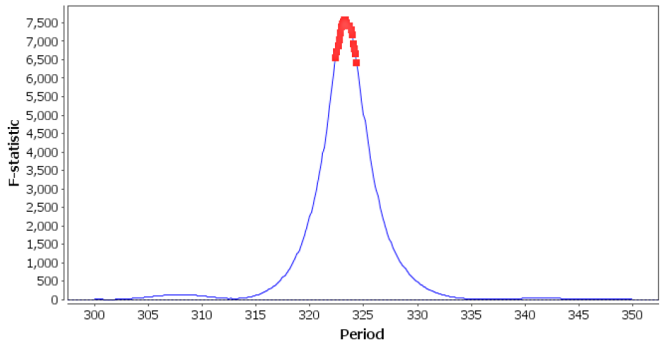

Figure 3. AoV Periodogram for S UMi (JD 2450000–JD 2459200).

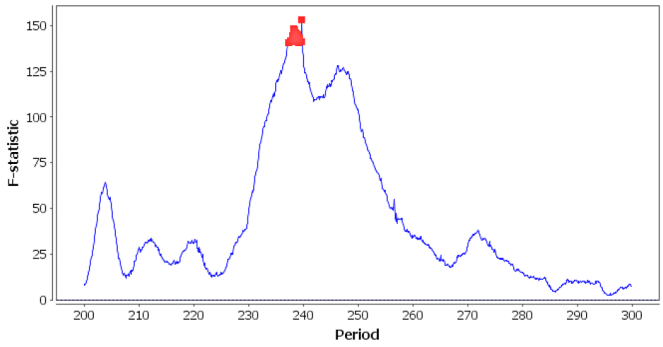

Figure 4. AoV Periodogram for T UMi (JD 2450000–JD 2459200).

A concentration of high F-statistic points, as depicted in Figure 3, indicates that the star is well-sampled, and that there is only one strong candidate period. Figure 4 depicts a periodogram with more noise, characteristic of semiregular stars. In these cases, the peak of the plot was confirmed by finding the period through the application of self-correlation studies, introduced in section 3.3. For example, the peak period in Figure 4 at approximately 240 days coincides with the period in the self-correlation plot of T UMi (Figure 5).

3.3. Self-correlation

To verify or suggest corrections and/or updates to the variability types of our subject stars (and as a tertiary form of period analysis), we developed a self-correlation algorithm, following the intuition of Percy and Kojar (2013), Percy and Mohammed (2004), and Percy and Ralli (1993). For all pairs of measurements in a given range of Julian Days, which total to $\binom{N}{2}$ pairs of (JD, magnitude in V), where N is the number of observations, we calculate Δt and |Δmagnitude| (Δmag), appending these $\binom{N}{2}/2$ values to arrays of Δts and Δmags. After deciding on an optimal "bin width" for each data set, which we found to be 10 days, all Δts that fall within that range are averaged, along with the corresponding Δmag values. We plot these averaged (Δt, Δmag) pairs in a self-correlation diagram.

Numerous changes in the period or shifts in amplitude of a subject star result in a self-correlation diagram with a non-constant amplitude. Rather than inspecting the light curves of such stars, we conduct a visual analysis of their self-correlation plots, as shown in Figures 5–7 and 13–14. A range of average Δt = 0 to average Δt = 1,000 is sufficient to detect trends in self-correlation amplitudes. As discussed in reference to our specific plots, the behavior of the plot changes noticeably when selecting different time periods with the same JD range and bin width.

The relative minima of self-correlation diagrams, in most cases, reflect primary pulsation periods for Mira stars, and often for SR variables as well, although such minima tend to be changing in average Δmag. We quantitatively confirmed the periods of the majority of our subject stars, with the exception of AU Cam, which we will discuss in section 4.4.

In some of our self-correlation diagrams, the final few peaks seem to exhibit irregular behavior. This trend is not due to intrinsic properties of the subject star, but is rather an artifact of running the algorithm; the frequency of Δt values decreases as Δt increases, and as such, Δmags are more sparse on the plots.

4. Results

All systems studied are listed in Table 1 with their GCVS variable type, most recently revised period and magnitude range listed in the VSX, periods determined through DC DFT and AoV analysis, and the magnitude range obtained from the light curve plots of the stars. Although the majority of our analyses provided confirmations of the VSX values in Table 1, we encountered numerous subject stars that exhibited deviations from the VSX data—particularly differences in period. We also make note of several trends or irregularities that we observed.

The stars with asterisked DC DFT periods exhibit one or more harmonic periods that are unit fractions of the fundamental period. RW And, TX Cam, and Y Cep have respective harmonic periods of 215.6, 279.9, and 166.9 days. X Cep has a harmonic of 267.0 days and a third harmonic of 178.9 days. These harmonics are not caused by actual pulsations of the star, but are rather high-frequency artifacts (Percy and Golaszewska 2020) due to the asymmetry of the light curve shape.

X UMi, although it has more than 2,000 visual and Johnson V band observations, has poorly dispersed data, as observations are clustered together, resulting in a light curve that lacks periodicity and consistency. However, after running both DC DFT and AoV analyses for different JD ranges, we arrived at period values consistent enough to suggest an update to X UMi's period in the VSX, from 388 days to 339 days.

Finally, T UMi, which we soon discuss in more depth, exhibited a period of approximately 237.5 days and a secondary pulsation mode with period 247.6 days, a substantial change from the period of 115.7 days listed in the VSX. Our period was confirmed by both the Fourier routine and AoV.

4.1. T UMi

Here we demonstrate the "optimal" self-correlation diagram of a well-observed SR variable—that is, almost perfectly periodic and having a steadily changing amplitude—T UMi. Corresponding with the decreasing magnitude in T UMi's light curve (Figure 8), the amplitude of the self-correlation plot in Figure 5 exhibits a decreasing trend, hinting at typical semiregular behavior. However, a decreasing self-correlation amplitude is not the sole indication of semiregularity. As we will discuss with regard to other SR-type stars, abnormal correlation diagrams—whether defined by a lack of periodicity or a changing amplitude—may also suggest semiregularity.

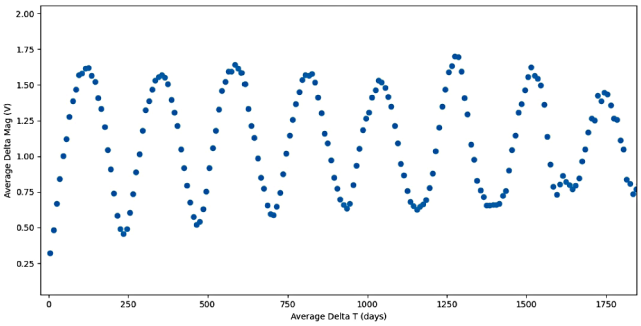

Figure 5. Self-correlation plot for T UMi (JD 2452000–JD 2454000).

4.2. R UMi

Figures 6 and 7 reflect the changing behavior of R UMi across varying Julian Day time scales. Such irregular periodicity, as is evident in R UMi's light curve in Figure 10, is characteristic of a semiregular variable star, confirming the VSX variability type of a general SR. In addition, the magnitude range decreases from 0.3–0.9 V to 0.3–0.65 V. Plots of additional Julian Day time shifts have been omitted for brevity, but generally confirm a decreasing average magnitude for R UMi. Though the upper plot reflects a clear primary period, confirmed by a brief glance at the star's light curve in Figure 10, the peaks in the lower plot suggest the potential presence of two pulsation modes.

However, both the primary and secondary periods are larger than the typical periods of Cep(B) or RR(B) stars, further confirming that the variability type of SR is the most likely classification.

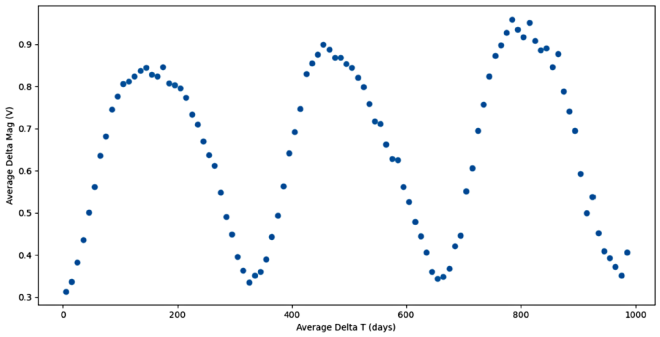

Figure 6. Self-correlation plot for R UMi (JD 2451000–JD 2452000).

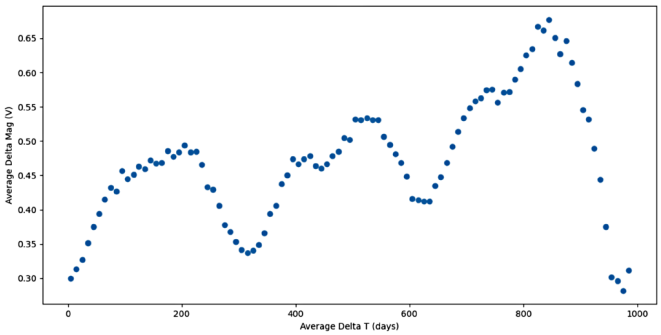

Figure 7. Shifted self-correlation plot for R UMi (JD 2452000–JD 2453000).

Table 1. Stars discussed in this study.

Name	*GCVS Type*	*VSX Period (days)*	*VSX Mag Range (V)*	*DC DFT Period (days)*	*AoV Period (days)*	*Mag Range (V)*
R And	M	409.2	5.8–15.2	407.4	409.4	5.7–15.4
RW And	M	430.0	7.9–15.7	431.1*	431.5	7.7–17.4
V And	M	256.4	9.0–15.2	257.3	258.2	15.4–18.4
AU Cam	SRA	366.0	10.0–10.7	363.5	363.7	9.0–11.4
R Cam	M	270.22	6.97–14.4	270.1	269.6	7.8–14.2
T Cam	M	369.3	7.2–14.4	375.9	375.8	7.3–14.4
TX Cam	M	558.7	7.8–16.9	559.8*	555.7	7.7–15.8
R Cas	M	430.5	4.7–13.5	435.3	433.2	3.7–14.2
S Cas	M	608.2	7.9–17.3	613.6	611.3	8.0–17.5
T Cas	M	440.0	6.9–13.0	444.1	442.5	7.3–12.3
W Cas	M	407.9	8.2–13.0	406.4	405.1	8.1–13.3
S Cep	M	484.4	6.6–12.5	482.3	482.0	6.1–11.5
T Cep	M	388.1	5.2–11.3	385.9	384.6	5.0–11.5
Y Cep	M	332.6	8.1–16.0	332.0*	333.6	8.0–15.5
X Cep	M	535.2	8.1–17.5	533.9	533.7	8.0–15.6
R Dra	M	245.6	6.7–13.2	247.5	247.5	5.9–14.0
RY Dra	SRA	300.0:	5.88–8.0	276.8	276.7	5.7–8.4
T Dra	M	422.2	7.2–13.5	420.5	422.5	8.4–14.0
U Dra	M	316.1	9.1–14.6	318.7	319.0	8.8–14.6
W Dra	M	278.6	8.9–15.4	286.6	287.0	9.0–15.8
R UMi	SR	325.7	8.5–11.5	324.3	324.4	8.2–11.5
S UMi	M	331.0	7.5–<13.2	323.9	323.3	7.4–13.0
T UMi	SR	115.7	7.8–15.0	237.5, 247.6	239.7	9.1–14.2
U UMi	M	330.9	7.1–13.0	324.1	323.9	7.4–12.5
X UMi	M	388.0	12.5–18.4**	339.2	338.8	11.5–16.1

Note: A single asterisk (*) denotes the presence of a harmonic period. Double asterisks (**) designate a magnitude range under photographic passband. The colon (:) is a symbol used by the VSX to indicate an uncertain value.

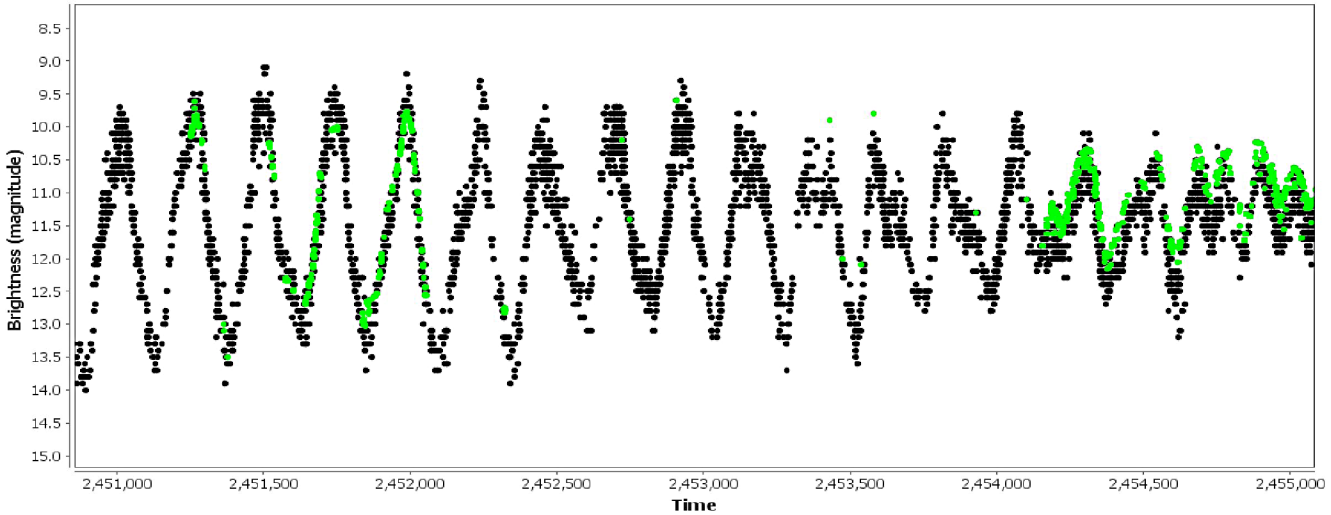

Figure 8. Light curve of T UMi generated from vstar, JD 2451000–JD 2455000.

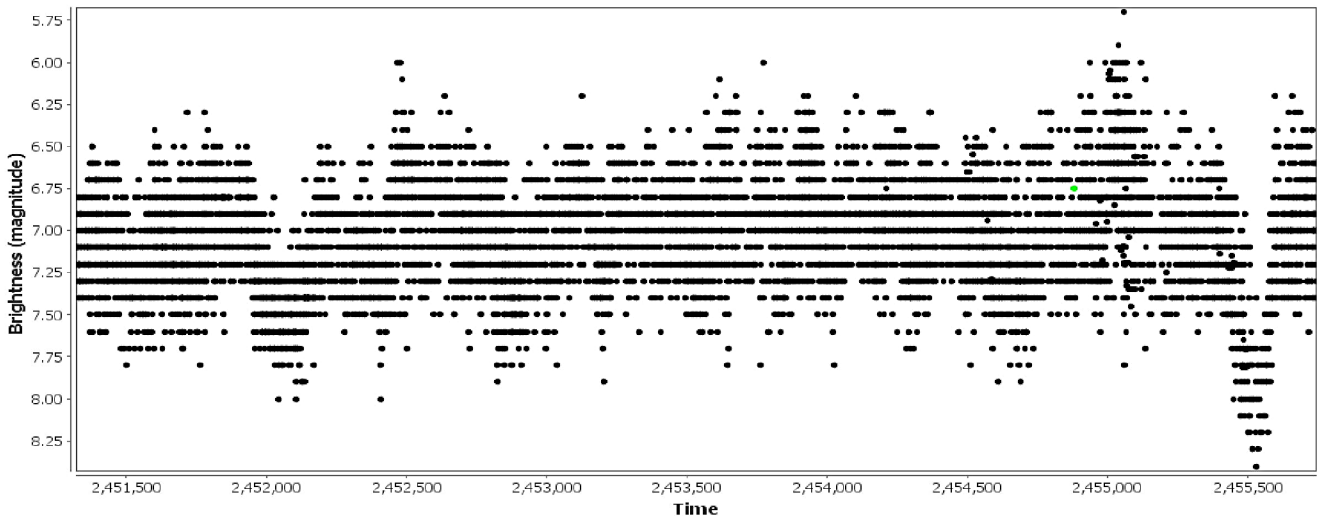

Figure 9. Light curve of RY Dra generated from vstar, JD 2451500–JD 2455500.

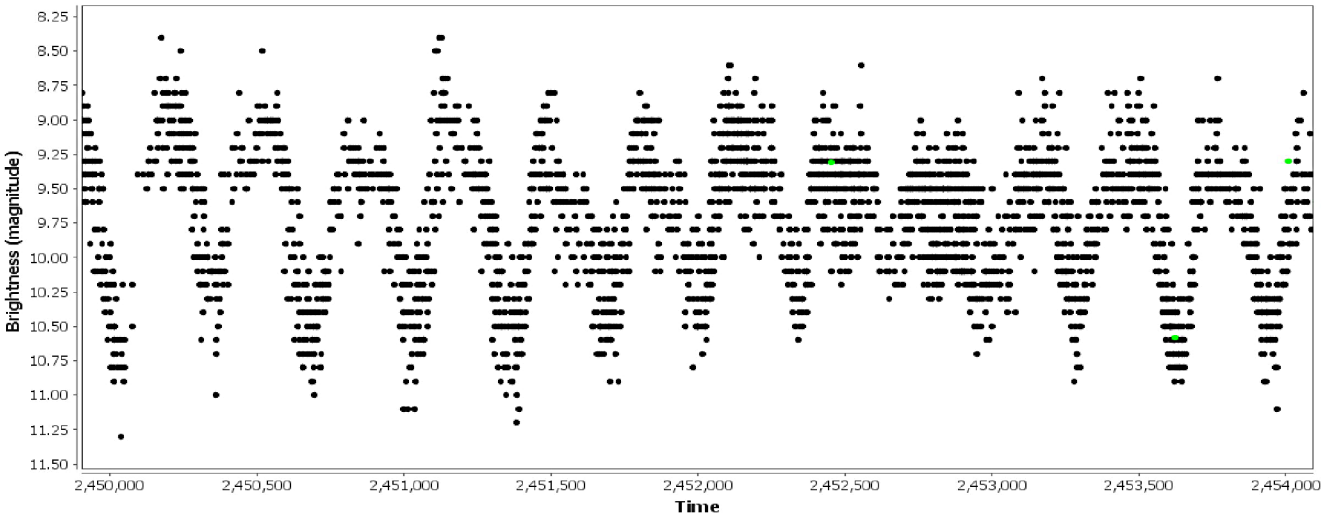

Figure 10. Light curve of R UMi generated from vstar, JD 2450000–JD 2454000.

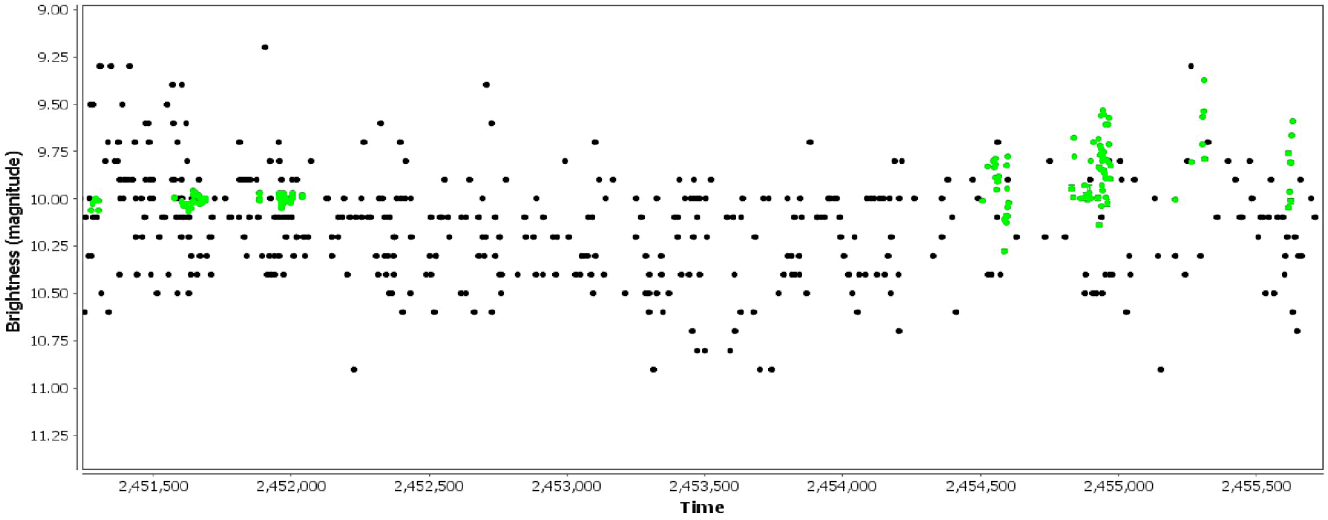

Figure 11. Light curve of AU Cam generated from vstar, JD 2451500–JD 2455500.

4.3. RY Dra

As depicted in Figure 12, RY Dra displays clear irregularity when compared to the previous self-correlation plots of SR and SRA stars, even over cycles of 6 periods. The self-correlation plot also suggests the presence of two or more pulsation modes, especially when considering its light curve (Figure 9), as there appear to be multiple maxima and minima per cycle. This behavior coincides with its classification as an SRB star. These stars are generally characterized by poorly defined periodicity and irregular changes. As in the case of R UMi, the self-correlation plots of various Julian Day time shifts display changing magnitude ranges. RY Dra has both increasing and decreasing magnitude ranges over longer Julian Day time scales, a behavior that agrees with that of its light curve.

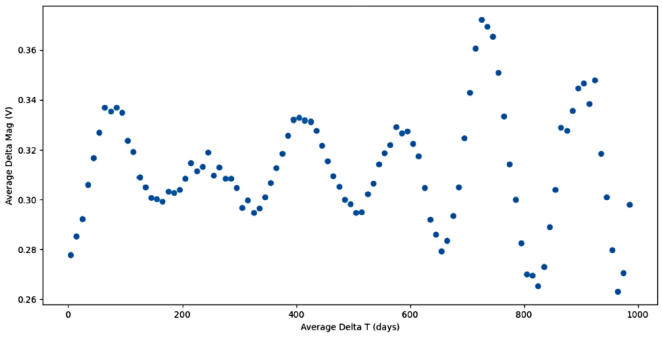

Figure 12. Self-correlation plot for RY Dra (JD 2453000–JD 2454000).

4.4. AU Cam

Vague periodicity can be seen in the light curve of AU Cam (Figure 11), and the self-correlation plot in Figure 13 even more irregular. The distribution of data points in AU Cam's light curve is relatively sparse, though this is not a sufficient indication of the star's variability type. However, the plot demonstrates a clear, gradual increase in Δmag, which is highly indicative of an SRA type variable star.

AoV and DC DFT analysis on AU Cam resulted in a period of 363.6 days. Upon a cursory glance, it appeared that this year-long period may have been a result of the seasonal Ceraski effect, briefly described by Percy *et al.* (2009). This effect causes a different perception of the magnitude difference between two stars due to the changing orientation of the star field throughout the year. The self-correlation diagrams of AU Cam further depict that the period of one year is likely spurious. Moreover, the DC DFT power spectrum exhibits a peak at a frequency of 0.000011 Hz with an amplitude nearly 6 times that of the 363.6-day period, similar to the behavior of the stars analyzed by Percy (2015). In accordance with Percy's conclusions, aliasing of AU Cam's VLF variability is the most likely cause of the one-year period.

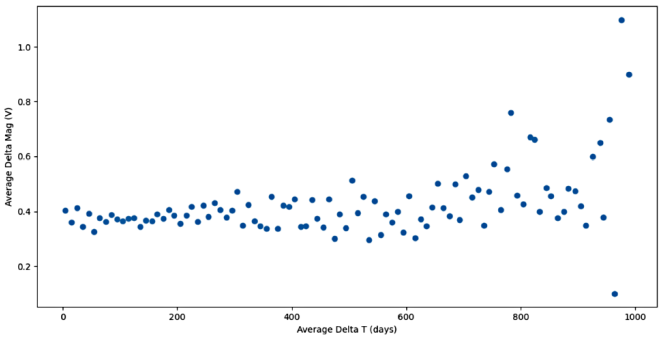

Figure 13. Self-correlation plot for AU Cam (JD 2453000–JD 2454000).

5. Conclusion

Our study supports the existing characterizations and key stellar attributes of most of the systems studied. These attributes include pulsation amplitude, GCVS variability type, and period, which we confirm via several analytical methods. The one standout case is T UMi, which appears to exhibit two pulsation modes that are, respectively, nearly 122 and 132 days longer than the VSX period. It is important to note that our proposed periods are not necessarily the most likely, as self-correlation was run on a larger JD range. Nevertheless, it is very likely that T UMi's period has increased appreciably since its last update in the VSX, and that the periods we arrived at are within an acceptable range.

Our self-correlation analysis provided no updates to the variability types of SR variables T UMi, R UMi, RY Dra, and AU Cam, though we emphasize the versatile nature of analyses of this sort. We also show how period and amplitude change through pulsation cycles, and how selecting different time scales reveals peculiar trends, specifically in the self-correlation plots of SR variables.

6. Acknowledgements

Both authors contributed equally to this work. We thank the observers and staff of the AAVSO for the data used in this research, as well as the developers of the VStar software package. We additionally relied on the International Variable Star Index database. We also thank Dr. John R. Percy and Dr. Adam W. Rengstorf for providing insight regarding period analysis with self-correlation, among other inquiries.

References

AAVSO. 2018, Variable Star Classification and Light Curves Manual, version 2.4, AAVSO, Cambridge, MA.

Benn, D. 2013, VStar data analysis software (http://www.aavso.org/vstar-overview).

Blackham, K. M. 2020, *J. Amer. Assoc. Var. Star Obs.*, **48**, 111.

Ferraz-Mello, S. 1981, *Astron. J.*, **86**, 619.

Kafka, S. 2021, variable star observations from the AAVSO International Database (https://www.aavso.org/aavso-international-database-aid).

Percy, J. R. 2015, *J. Amer. Assoc. Var. Star Obs.*, **43**, 176.

Percy, J. R., Esteves, S., Lin, A., Menezes, C., and Wu, S. 2009, *J. Amer. Assoc. Var. Star Obs.*, **37**, 71.

Percy, J. R., and Fenaux, L. 2019, *J. Amer. Assoc. Var. Star Obs.*, **47**, 202.

Percy, J. R., Golaszewska, P. 2020, *J. Amer. Assoc. Var. Star Obs.*, **48**, 165.

Percy, J. R., Kojar, T. 2013, *J. Amer. Assoc. Var. Star Obs.*, **41**, 15.

Percy, J. R., and Mohammed, F. 2004, *J. Amer. Assoc. Var. Star Obs.*, **32**, 9.

Percy, J. R., and Qiu, A. L. 2019, *J. Amer. Assoc. Var. Star Obs.*, **47**, 76.

Percy, J. R., Ralli, J. A., and Sen L. V. 1993, *Publ. Astron. Soc. Pacific*, **105**, 287.

Samus, N. N., Kazarovets, E. V., Durlevich, O. V., Kireeva, N. N., and Pastukhova, E. N., 2017, *Astron. Rep.*, **61**, 80, *General Catalogue of Variable Stars: Version GCVS 5.1* (http://www.sai.msu.su/gcvs/gcvs/index.htm).

Watson, C., Henden, A. A., and Price, C. A. 2014, AAVSO International Variable Star Index VSX (Watson+, 2006–2014, https://www.aavso.org/vsx).